

**Inducing a sign inversion in one state of a two-state superposition using ultrafast pulse shaping**Joshua B. Ballard,<sup>1,\*</sup> Alan N. Arrowsmith,<sup>1,\*</sup> Lutz Hüwel,<sup>1,†</sup> Xingcan Dai,<sup>2</sup> and Stephen R. Leone<sup>1,\*</sup><sup>1</sup>*JILA, National Institute of Standards and Technology and University of Colorado, Department of Chemistry and Biochemistry, and Department of Physics, Boulder, Colorado 80309-0440, USA*<sup>2</sup>*Department of Physics and Lawrence Berkeley National Laboratory, University of California, Berkeley, California 94720, USA*

(Received 21 May 2003; published 22 October 2003)

An ultrafast pulse shaping scheme is presented that transiently modifies a two-state superposition on the  $E \ ^1\Sigma_g^+$  curve of the lithium dimer. At short time delays, the wave-function amplitude of one of the states is forced to undergo a sign change, while the sign of the second state is programmed to remain static, analogous to the operation of a quantum-computational  $Z$  gate. This is observed as a  $\pi$  phase shift in the time-dependent wave-packet signal for pump-probe delays  $<1.5$  ps, relative to longer time delays, greater than 2.5 ps. This shift in sign is accomplished by taking advantage of the separability of the resonant and nonresonant light field effects in the creation of the excited-state wave function. The results show that, for a single state, the resonant and nonresonant light field effects can either be added or subtracted to create the total time evolution of the excited-state wave-function coefficient. If the nonresonant contributions are subtracted from the resonant ones at a time delay when the nonresonant term dominates, then for a short time the excited-state coefficient will have a sign opposite to that at long time, where the resonant term dominates. A desired phase function is derived to produce the opposition in sign of resonant versus nonresonant contributions, and the experimental transient  $Z$ -gate matrix elements are quantified.

DOI: 10.1103/PhysRevA.68.043409

PACS number(s): 42.50.Md, 33.80.Eh, 32.80.Qk, 82.53.Hn

**I. INTRODUCTION**

The study of coherent control to manipulate molecular systems has generated numerous tools that can be useful for directing a system under optical, especially ultrafast, excitation [1–13]. The tools of coherent control may be applicable to quantum computing, where superpositions of quantum states, or qubits, are used to perform computational operations [14]. Crucial to being able to perform quantum operations is the ability to manipulate individual states within qubits. Basic computations have been performed on spin systems using nuclear magnetic resonance with considerable success [15–18]. Optically manipulated systems using trapped atoms and ions also show promise for quantum computation by using narrow-bandwidth lasers to resonantly control particular transitions between states [19,20]. Wide-bandwidth, ultrafast pulses have been proposed as a means to implement quantum-computational operations using the relatively dense states inherent to single quantum dots and even molecules [9–13]. Given the relatively short decoherence times ( $<100$  ns) of these more complex systems, the use of ultrafast laser sources is valuable to perform sufficient numbers of operations for meaningful computations.

This article explores a mechanism for using weak-field, ultrafast pulse-shaping techniques and nonresonant excitation to manipulate individual states in a molecular superposition, specifically multiple rotational states in an excited electronic state of the lithium dimer. As an example of using

nonresonant frequencies to control the amplitude of molecular rotational states, a transient  $Z$  gate is implemented. Using an ultrafast pulse with sufficient bandwidth to encompass resonant transitions to two excited states, one state of the two-state superposition will have its sign unchanged in time while the other will undergo a transient sign inversion. Since the state that undergoes sign inversion is initially a transiently prepared state, this operation is not necessarily temporally reversible, so it cannot be used for actual computation. Nevertheless, the results illustrate the possibilities of using optical pulse-shaping techniques for individual state manipulation.

Earlier, it was shown that resonant frequencies can be used to control the phases of states involved in a wave packet [21,22], and it was also shown that nonresonant frequencies can be used to transiently manipulate the absolute amplitude of resonant transitions, even in a weak field [23,24]. One additional aspect of transient, ultrafast control of wave-packet phases has not been demonstrated: i.e., the transient phase of a wave packet can be controlled by using nonresonant frequencies. In any first-order process, though, the final wave-packet phase and amplitude at long times are determined by the resonant frequencies, as expected [2].

To demonstrate this change in phase, we first selectively excite a single rovibrational state in the first excited electronic state ( $A \ ^1\Sigma_u^+$ ) of the lithium dimer ( $v_A=11, J_A=28$ ). Next, using an ultrafast pulse we weakly excite a two-state rotational superposition on the  $E \ ^1\Sigma_g^+$  curve ( $v_E=9, J_E=27, 29$ ). We photoionize this superposition with a time-delayed probe pulse. Depending upon the relative angle of linear polarization of the pump and probe pulses, we can observe either a coherence-free population signal [at the magic angle ( $54.7^\circ$ ) of relative pump and probe polarizations] or a full signal including the coherent quantum beat (at parallel pump and probe polarizations) [4]. Using pulse shap-

\*Present address: Department of Chemistry and Department of Physics and Lawrence Berkeley National Laboratory, University of California, Berkeley, CA 94720, USA.

†Permanent address: Department of Physics, Wesleyan University, Middletown, CT 06457, USA.

ing, we divide the ultrafast pulses into multiple spectral regions: a resonant region around each transition frequency, and nonresonant regions above and below each resonant region. By defining the excitation spectrum in this way, we are able to separate the resonant and nonresonant contributions that produce each state in the wave packet and independently manipulate these contributions.

We show in this article that the wave-packet phase can be induced to undergo a  $\pi$  phase shift at time zero relative to long times. Assuming that one contributing state in the superposition has a constant phase at all times so as to act as a reference state, the signal shows a change in sign because of a transient sign inversion of the second state. This dynamical effect is accomplished by summing nonresonant and resonant contributions for one state while subtracting the nonresonant from the resonant contributions for the second state. The amplitudes of the relative contributions of each effect are also adjusted so that the nonresonant contribution dominates at short times but naturally disappears at long times. This process of inverting the sign of one state of a superposition while leaving the second unaltered is characteristic of a quantum-computational  $Z$  gate, which in this case is constructed to operate on a transient state.

This example of controlling the dynamic phase of a wave function in the weak-field regime provides a rather clear illustration of the limitations and possibilities of precise control of molecular systems. As long as the intensity of the electric field is weak enough to disregard intensity-dependent Rabi oscillations, pure phase shaping of the ultrafast pulses fully controls the dynamics of the effects observed. In Sec. II, a theoretical framework for these experiments is presented using first-order perturbation theory. In Sec. III a description of the experimental apparatus is presented as well as a categorization of the resonant and nonresonant effects that are used as tools in these experiments. Finally, the experimental results are presented, discussed, and quantified in Sec. IV.

## II. THEORY

This article develops a method to induce a transient sign change in one state of a two-state superposition, or wave packet. The wave packet consists of two states that are excited coherently, so that

$$\Psi'(t) = c_0(t)|0\rangle + c_1(t)|1\rangle + c_2(t)|2\rangle, \quad (1a)$$

where  $c_0(t)$  is the launch-state wave-function amplitude,  $c_1(t)$  and  $c_2(t)$  are the complex excited-state wave-function amplitudes to be described below with  $c_1(t), c_2(t) \ll c_0(t)$ , and  $|0\rangle$ ,  $|1\rangle$ , and  $|2\rangle$  are the rovibrational wave functions in the superposition. The detection scheme is sensitive only to  $|1\rangle$  and  $|2\rangle$ , so the effective wave packet can be reformulated as

$$\Psi(t) = c_1(t)|1\rangle + c_2(t)|2\rangle. \quad (1b)$$

As described previously [21,24], the photoionization signal using parallel, linear pump and probe polarizations can be written as

$$S(t) \equiv |c_{pr_1}|^2 |c_1(t)|^2 + |c_{pr_2}|^2 |c_2(t)|^2 + 2|c_{pr_1}c_{pr_2}| |c_1(t)c_2(t)| \cos[\Delta\omega t + \Delta\varphi(t)], \quad (2)$$

where  $c_{pr_1}$  and  $c_{pr_2}$  are constants related to the probe step and will be assumed to have a value of unity (see [25]); the energy separation of the particular states chosen,  $\Delta\omega$ , is  $42 \text{ cm}^{-1}$  (1.5 THz); and  $\Delta\varphi(t)$  is the relative phase between the wave-packet states at time  $t$ . It has been shown that for a probe polarization aligned at the magic angle with respect to the pump polarization (“magic-angle probe”), the coherent oscillation (quantum beat) is completely suppressed, leaving only the  $|c_1(t)|^2 + |c_2(t)|^2$  part of the signal [24].

Consequently, the difference between the parallel and magic-angle signals yields only the quantum beat. The probe pulse is relatively weak, so the multiphoton ionization pathway from the launch state ( $c_{pr_0}$ ) is also weak. Since  $c_{pr_0} \ll c_{pr_1}, c_{pr_2}$ , all launch-state terms are left out of the signal, and the time-dependent signal shows only the dynamics of the excited states.

In these experiments, the probe step consists of an ultrafast pulse of a different color (645 nm) from the pump pulse (801 nm) [24], so as to avoid any ambiguities in contributions to the signal when the probe comes before the pump. With the 645 nm probe pulse, the probability for a probe-pump (i.e.,  $t < 0$ ) ionization pathway is below the noise level, allowing time-dependent ionization to occur only at positive time delays. This allows the transient populations and coherent oscillations to be measured reliably around  $t = 0$ .

In the weak-field limit, first-order time-dependent perturbation theory can be used to describe the single-photon absorption. As shown before [23,24], the excited-state amplitude for a single state can be approximated for positive time  $t$  by the frequency domain expression

$$c_n(t) \propto \bar{\varepsilon}^*(\omega_{eg}) - \frac{i}{\pi} \wp \int_{-\infty}^{\infty} \frac{\varepsilon(\omega) \exp[i(\delta)t]}{\delta} d\omega, \quad (3)$$

where  $\bar{\varepsilon}^*(\omega_{eg})$  is the amplitude of the electric field at the transition frequency,  $\varepsilon(\omega)$  is the amplitude of light at frequency  $\omega$ ,  $\delta = \omega - \omega_{eg}$  is the detuning, and  $\wp$  is the Cauchy principal value. The first term in Eq. (3) is the resonant term, which determines the wave-packet behavior as  $t$  approaches infinity, and the second term is the nonresonant term and can be seen only transiently. In the absence of any phase manipulation (i.e., transform-limited pulses), the spectrally integrated nonresonant term will be greatly diminished for all  $t$ , since the time-dependent contributions for  $\omega > \omega_{eg}$  are  $\pi$  out of phase with respect to the contributions for  $\omega < \omega_{eg}$  [26,27]. Additionally, the  $i/\pi$  leading factor of the nonresonant term causes the nonresonant contribution to be  $\pi/2$  out of phase with respect to the resonant term. To compensate for these spectroscopic phase shifts, a phase of  $+\pi/2$  and  $-\pi/2$  must be added to the nonresonant frequencies above and below  $\omega_{eg}$ , respectively, to obtain the maximum transient amplitude coefficients. Additionally, the  $1/\delta$  dependence of the nonresonant term shows that the most influential nonresonant

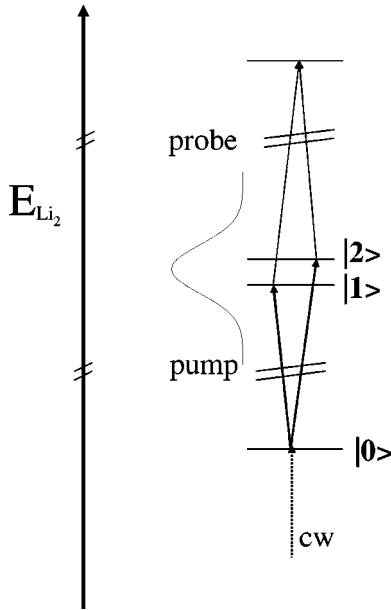


FIG. 1. States involved in excitation scheme. A cw laser excites from the  $X^1\Sigma_g^+$  electronic curve to a pure launch state (state  $|0\rangle$ ) in the  $A^1\Sigma_u^+$  electronic state. A wide-bandwidth 801 nm ultrafast pump pulse excites a superposition of states (states  $|1\rangle$  and  $|2\rangle$ ) in the  $E^1\Sigma_g^+$  electronic state, which is subsequently ionized by a time-delayed 645 nm ultrafast probe pulse.

frequencies will be those with the smallest detuning. Notice that these effects result in a  $c_n(t)$  that is primarily real at  $t=0$  and  $\infty$  under the conditions imposed in these experiments. The manner in which the various contributions interact is explored in the next section to demonstrate how to change the wave-function sign.

In this article, a transformation of the qubit in Eq. (1b) is empirically equivalent to a quantum-computational Z gate. Using a matrix formulation, the action of the ultrafast pulse on the prepared superposition transforms the system as a single qubit Z gate:

$$\begin{bmatrix} c_1(f) \\ c_2(f) \end{bmatrix} \approx \begin{bmatrix} 1 & 0 \\ 0 & -1 \end{bmatrix} \begin{bmatrix} c_1(i) \\ c_2(i) \end{bmatrix}. \quad (4)$$

First, a superposition is prepared such that at  $t=0.0$  ps the two excited states have amplitudes of opposite sign so that  $c_1 \approx 1$ , and  $c_2 \approx -1$ . The electric field then drives the system so that the sign of  $c_2$  changes, leaving  $c_2=1$  at long times.

### III. EXPERIMENT

The lithium sample is contained in a heat pipe at 1050 K and is photoionized by a three-step excitation process, as shown in Fig. 1 [28,29]. An overview of the laser system is given below, but details can be found in previous work [24]. In this experiment, a narrow-bandwidth continuous-wave (cw) laser, an amplified ultrafast system, and an optical parametric amplifier (OPA) are used, and all but the OPA are pumped by a 27 W argon ion laser. The frequency of the cw laser is tuned to a specific  $A^1\Sigma_u^+ \leftarrow X^1\Sigma_g^+$  resonance (606.954 nm) of  $\text{Li}_2$ , producing a pure launch state ( $v_A$

$=11, J_A=28$ ). The ultrafast regenerative amplifier produces 200 fs pulses at a 200 kHz repetition rate, with an 801 nm central wavelength and  $\sim 8$  nm [full width at half maximum (FWHM)] bandwidth. These ultrafast pulses are split into two beams, with 25% of the light becoming the pump pulse and 75% of the light used to pump the OPA to obtain the probe pulse. The resulting 45 mW OPA output at 200 kHz is a train of nearly transform-limited pulses with a 200 fs FWHM pulse width and a central wavelength of 645 nm. The OPA output is variably time delayed relative to the pump pulse via a precision delay stage.

To shape the pump pulse, it is sent through a dispersion-free pulse shaper [30,31]. In the pulse shaper's Fourier plane, a liquid-crystal spatial light modulator (SLM) is used to shape the spatially dispersed pump light by independently attenuating and/or applying phase to up to 128 individual frequency components (SLM pixels) of the pump light. The central frequencies imaged onto the SLM pixels are spaced by approximately  $4 \text{ cm}^{-1}$  with a single-frequency spot size of approximately 1.7 pixels. In the present case, the 8 nm (or  $124 \text{ cm}^{-1}$ ) FWHM pulses are imaged onto the SLM to achieve a bandwidth of about 30 pixels FWHM. Further studies of the spectral contributions to the signal are done by utilizing the ability of the SLM to attenuate frequencies in addition to manipulating phase. By attenuating all of the light on a single pixel and monitoring the decrease in total photoionization, it is possible to quantify the contributions of various spectral components of a shaped or unshaped pulse [21]. Typically, this method is used for calibration purposes; when a resonant frequency is attenuated, the total photoionization goes down. This procedure can also be applied to phase-shaped pulses, as will be explored later.

The cw laser and pump and probe pulses produce photoions in the center of the heat pipe between two parallel stainless steel plates separated by 1 cm with a 5 V potential applied. The cw light is optically chopped, and the resulting current is detected with a lock-in amplifier that is synchronized to the cw modulation.

To investigate phase mask effects, the available spectrum is defined as consisting of two spectral channels separated at the energetic midpoint between the two resonant transitions. A global phase offset can be added to the channel for state  $|2\rangle$  in order to control the long-time wave-packet phase [24]. Within each channel, i.e., for each state, resonant and non-resonant contributions to the excited-state wave-function coefficient are independently controlled. See Fig. 2 for one phase mask that is used to add the resonant and nonresonant contributions of the excited-state coefficients together, along with the corresponding observed time domain evolution. In Fig. 2(a), it is shown that a small bandwidth region around each resonance ( $\sim 8 \text{ cm}^{-1}$ ) is assigned a phase halfway between the positive and negative detuned nonresonant frequencies. The effect of these narrow-bandwidth resonant regions is a nearly monotonic increase in the photoionization signal, as shown by the triangles in Fig. 2(b). This will be referred to as the resonant contribution. The applied  $\pi$  phase shift between positive and negative detuned frequencies around each resonance compensates for the intrinsic spectroscopic  $\pi$  phase shift of the nonresonant contributions above

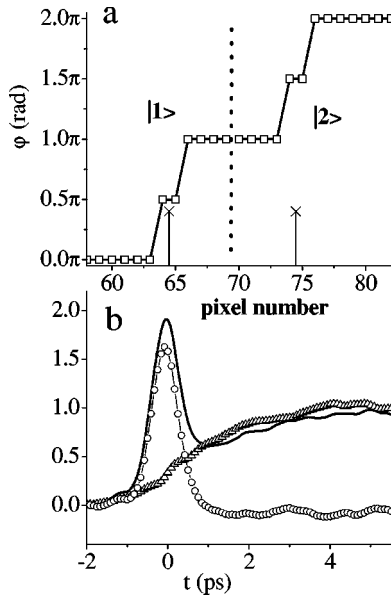


FIG. 2. Phase-shaped population transfer traces. (a) Phase mask used to maximize population transfer at  $t=0.0$  ps. The applied phase mask is given by  $\square$ , and resonances are marked with  $\times$ . The applied phase masks near each resonance (i.e., in each channel) are identical, assuring that both states follow the same excitation pathway, with a global phase offset of  $\pi$  rad for state  $|2\rangle$ . (b) Magic-angle traces using the applied phase mask of (a). The solid line represents the total population transfer signal, the  $\triangle$  shows the resonant-only contribution, and the  $\circ$  gives the nonresonant contribution, which is just the difference between the two traces.

and below the resonances. This allows the nonresonant contributions to cooperate on short time scales, as seen by the circles in Fig. 2(b). The solid line in Fig. 2(b) shows  $|c_1(t)|^2 + |c_2(t)|^2$ , which has been normalized. Assuming that the cross-talk between control channels for the two coefficients is insignificant [24], which is achieved when the two resonances are spaced far apart energetically,  $|c_1(t)|$  is approximately equal to  $|c_2(t)|$ . Therefore, the solid line is  $2|c_1(t)|^2$ . By taking the square root of the signal and renormalizing, a measure of each coefficient is obtained. This signal shows that at the times of interest in this article,  $t=0$  and  $\infty$ ,  $|c_1(t)|=1.4$  and  $1.0$ , respectively. This information will be used later to quantify the manipulations of the coefficient  $c_2(t)$ .

Figure 3 is a schematic diagram of the calculated *amplitude* of the excited-state coefficients [i.e.,  $c_n(t)$ , not  $|c_n(t)|^2$ ], based on parameters from the square root of the data from the cooperative signal described above. Also shown is an experimental realization of the photoionization signals for a single coefficient [the second level is not excited and the signal is proportional to  $|c_1(t)|^2$ ]. These resonant and nonresonant contributions can add to yield the amplitude of  $c_n(t)$ , and they can also be subtracted. This is done by multiplying either the resonant or nonresonant contribution by  $-1$ . In the complex plane, multiplication by  $-1$  is identical to the addition of  $\pi$  phase, which is accomplished by the application of  $\pi$  phase to the appropriate pump wavelengths. In these experiments, the state  $|1\rangle$  is manipulated to

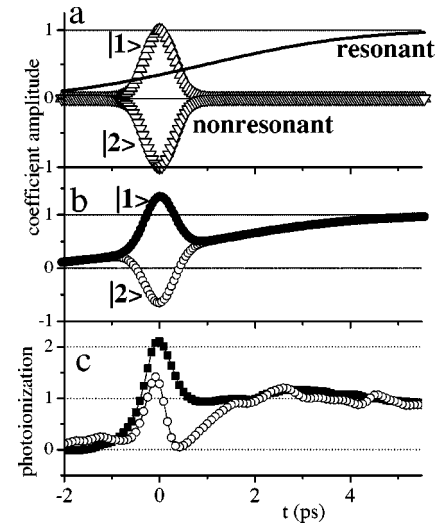


FIG. 3. Schematic resonant and nonresonant interaction scheme for inducing sign inversion. (a) Schematic resonant and nonresonant contributions to the population transfer. The solid line is the resonant contribution time shifted by  $1.0$  ps. The  $\triangle$  and  $\nabla$  reflect the nonresonant contribution for states  $|1\rangle$  and  $|2\rangle$ , respectively, when inducing a sign inversion. (b) Sum of resonant and nonresonant contributions to the excited-state coefficient evolution from (a).  $\bullet$  shows the time evolution for state  $|1\rangle$ , and  $\circ$  shows the time evolution for state  $|2\rangle$ . (c) Experimental photoionization traces for a single state with a phase mask that adds the resonant and nonresonant contributions ( $\blacksquare$ ), and a phase mask that subtracts the resonant and nonresonant contributions ( $\circ$ ). The photoionization signal correlates with the square of the amplitude coefficients.

be a sum of the resonant and nonresonant contributions with the same sign, while state  $|2\rangle$  consists of a difference of such contributions. Since the coefficient for  $|2\rangle$  reflects a difference, the absolute amplitude of this negative coefficient can be increased in one of two ways: by increasing the negative part or by decreasing the positive part. To decrease the positive contribution [solid line in Fig. 3(a)], the resonant contribution is time shifted by  $1.0$  ps by applying a simple linear phase mask to the resonant regions. To demonstrate these addition and subtraction effects experimentally on a single excited state, phase masks with nonresonant effects added or subtracted from resonant were applied to a pulse exciting the ( $v_E=7, J_E=39$ ) state, and the results are shown in Fig. 3(c). The light near state ( $v_E=7, J_E=41$ ), spaced over  $62\text{ cm}^{-1}$  away, was attenuated to make sure that it was not excited—so that  $c_2(t)=0$ . Excitation with the phase mask with the resonant and nonresonant parts added together shows the expected transient peak at  $t=0.0$  ps. Excitation with the phase mask that subtracts the nonresonant from the resonant contribution shows that the photoionization goes nearly to zero at  $0.42$  ps. It is at this time that the sign of the coefficient inverts and the wave-function phase quickly changes. These traces show the total photoionization, so they are proportional to  $|c_n(t)|^2$ , but it is quite clear from the data that excitation with the phase mask that subtracts the nonresonant part from the resonant part causes the excited state to go through a significant change.

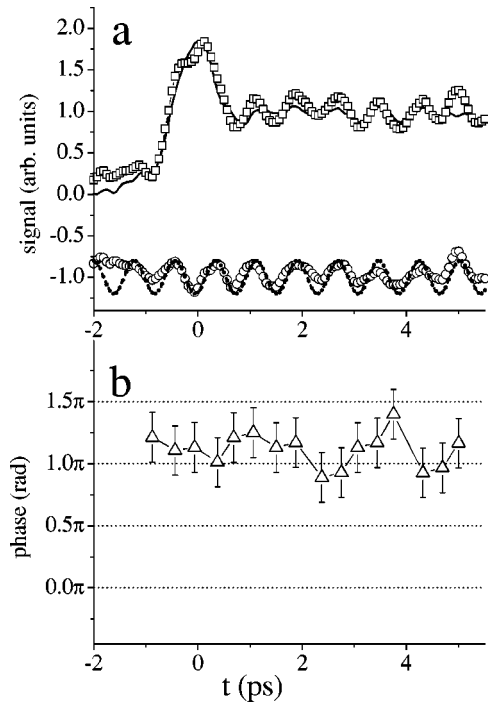


FIG. 4. Phase evolution using the same functional form of phase mask for each resonance. (a) Pump-probe signals using phase mask of Fig. 2. Parallel pump-probe polarization ( $\square$ ) and magic-angle pump-probe (solid line) traces are shown on the top. The small oscillations in the solid line are a result of residual ellipticity in the pump polarization. Also shown is the coherence-only signal ( $\circ$ ) as well as a single-cosine fit (dotted line). The coherence-only signal and fit have been vertically offset for visibility. (b) Instantaneous wave-packet phase. The maxima and minima of the coherence-only signal are compared to the fit to generate the instantaneous phase. The wave-packet phase remains relatively constant from the onset of the signal until long times.

#### IV. RESULTS AND DISCUSSION

To serve as a reference, a case where the dynamics of the population transfer are controlled identically for both states involved in the wave packet is shown in Fig. 4 (see [24]). Here, the resonant and nonresonant contributions to the signal are added together for both states  $|1\rangle$  and  $|2\rangle$ . The upper part of Fig. 4(a) shows that there is a peak in the transient populations of the excited states at  $t=0.0$  ps. The difference between the full signal and the population-only signal yields purely the coherence signal, which is shown as the circles in the lower part of Fig. 4(a). Notice that the coherence signal appears only after the excited-state coefficients become non-zero, and that it has an overall temporal phase of  $1.1\pi$  rad in this case. The amplitude of the coherent oscillation is smaller than the amplitude of the incoherent ionization due to “amplitude filtering” of the coherence signal [21]: for a coherence to be seen the interfering states must share not only a common launch state but also a common final state. Still, the phase information in the coherent oscillation remains largely unaffected by the amplitude of the coherence signal.

To show that the phase of the wave-packet oscillation remains constant during the population transfer process, the signal up to 6.0 ps pump-probe delay was compared to a

cosine wave that is generated to fit the coherence signal between  $t=6$  and 30 ps. The signal is fitted only at times after 6 ps to avoid potential uncertainties introduced by a changing wave-packet phase during the population transfer process. The maxima and minima of the coherence signal are compared to the fit, and the time offset of each peak relative to the fit is used to determine the instantaneous phase, plotted in Fig. 4(b). As is evident in Fig. 4(b), the experimental trace matches the fit with a phase of  $1.1\pi$  and a standard deviation of  $\pm 0.14\pi$  rad over all time delays up to 6 ps. This comes as no surprise, since no effects have been introduced to change the instantaneous phase of the wave packet.

The case of subtracting the nonresonant contributions from the resonant contribution is the main point of this article and is shown in Fig. 5. The phase mask that is used to induce a sign change in state  $|2\rangle$ , including the time shifting of the resonant contributions, is shown in Fig. 5(a). Note that the phase applied to the nonresonant contributions around  $|1\rangle$  is not changed from the additive case, as shown in the previous section. In contrast, the phase applied to the nonresonant contributions around  $|2\rangle$  is inverted; the nonresonant contributions have an additional  $\pi$  phase shift relative to the resonant ones, which is equivalent to a multiplication by  $-1$ , as explained previously. The corresponding signal traces from Fig. 5(b) show the expected population peak around  $t=0.0$  ps, just as when the contributions were added together. Note that this trace must remain positive, since the observed signal is a sum of squares for *both* states  $|1\rangle$  and  $|2\rangle$ . A critical difference in this case occurs in the coherence-only portion of the signal, which contains information about the wave-function sign. In Fig. 5(b) it is apparent that around  $t=0.0$  ps the quantum beat portion of the signal exhibits a transient phase of  $\sim\pi$  even though the relative phase between the resonant frequencies is 0.0 rad. This is caused by the nonresonant frequencies and their effect on the transient wave-function coefficients. The instantaneous phase graph of Fig. 5(c) displays a  $\pi$  phase shift in the region around  $t=0.0$  ps relative to  $t>2.0$  ps. This shows that there is indeed a temporally dynamic phase of one state in the wave packet relative to the other. In fact, it shows that the sign of one state has changed temporarily relative to the other.

A full discussion of the effects observed here cannot be made without a brief mention of the nonidealities at play in this pulse-shaping scheme. As was mentioned earlier, the resonant contribution to the signal was shifted by 1.0 ps to a more positive time to minimize the interactions between it and the nonresonant contributions. An example where the nonresonant contribution to the signal is not shifted in time is shown in Fig. 6. It is quite clear in this figure that the phase at  $t=0$  deviates substantially from either the 0 or  $\pi$  phase. The dynamics at play here are highly sensitive to the positions of the resonances relative to the demarcations between those spectral regions treated as “resonant” and “nonresonant.” If the actual resonance is not perfectly centered within the “resonant” portion of the selected region, there are variable amounts of positive and negative detuned wavelengths that have no compensating phase added. The net effect of this is that the instantaneous phase of the nonresonant contribution is not necessarily zero or  $\pi$ . When this nonideality

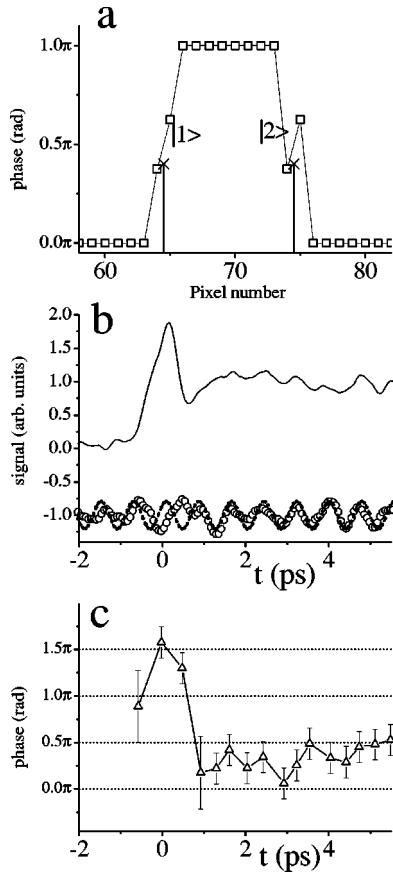


FIG. 5. Sign inversion wave-packet data. State  $|1\rangle$  is programmed to behave the same as in Fig. 4, but state  $|2\rangle$  is programmed to change sign. (a) Phase mask applied to induce sign inversion. The applied phase is given as  $\square$ , and the resonances are given by  $\times$ . The slight linear phase added to the resonant portion of the spectrum time shifts the resonant contribution. Notice that the relative phase between resonances is  $0.0$  rad. (b) Pump-probe signals using the phase mask of (a). Population transfer (solid line) trace is shown in addition to the coherence-only signal ( $\circ$ ) as well as a single-cosine fit (dotted line). The coherence-only signal and fit have been vertically offset for visibility. (c) Instantaneous wave-packet phase from onset of excited-state population. The wave-packet phase undergoes a  $\pi$  shift from  $t=0.0$  to  $t>1.0$  ps. The data points with larger error bars represent time delays where the coherent oscillation amplitude is small.

interacts with the transiently prepared state, there can be a large shift in instantaneous phase, as demonstrated in Fig. 6(b). For a single state [see Fig. 3(c)], the position of the resonant frequency can be tuned with subpixel precision by translating the SLM in the Fourier plane of the pulse shaper. In the case of two states, the relative spacing between resonances is fixed (at 10.7 pixels in this case), preventing the simultaneous placement of both resonances in the very center of the “resonant” bands. For this reason, the instantaneous phase is most predictable when the resonant and non-resonant contributions are separated in time.

Around  $t=0.0$  ps, when the sign of the wave function for state  $|2\rangle$  is inverted from that expected for the purely resonant phases, there is a certain degree of destructive interference in the contributions to the signal. By attenuating spe-

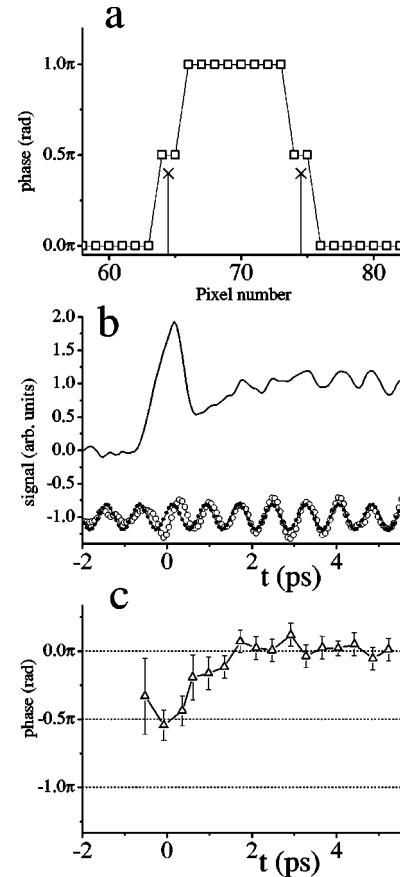


FIG. 6. Sign inversion wave-packet data without time shifting the resonant contribution. All symbols are the same as in Fig. 5. (a) Applied phase mask. (b) Pump-probe traces. The coherence-only signal and fit have been vertically offset for visibility. Notice the deviation in instantaneous phase away from the  $0$  or  $\pi$  phase at short times. Also notice that the coherent oscillation ( $\circ$ ) persists after its first appearance, in contrast to the small-amplitude oscillation at  $1.0$  ps in Fig. 5. (c) Instantaneous wave-packet phase.

cific individual frequencies of the shaped pulses, a measure of the relative contributions of the various spectral contributions can be made. The traces shown in Fig. 7 illustrate destructive interference at play around  $t=0.0$  ps for state  $|2\rangle$ . The data were acquired by setting the pump-probe delay to a specific value, either  $6.0$  or  $0.0$  ps, with either unshaped or shaped pulses, respectively, and attenuating the light imaged onto one pixel at a time. In the transform-limited case, at  $6.0$  ps, attenuating a contributing wavelength of light decreases the photoionization signal, and the wavelengths of light with the greatest contribution to the signal cause the greatest decrease in the photoionization. In Fig. 7, the relative contribution to the photoionization is plotted. The circles show the relevant pixels using unshaped pulses at a pump-probe time delay of  $6.0$  ps. The trace shows a narrow bandwidth of contributing pixels, as one would expect since resonant frequencies determine the ultimate behavior of each state at long times in the weak-field limit. The approximately two-pixel bandwidth is primarily an effect of spot size on the pulse shaper and not the intrinsic transition bandwidth. The squares show the spectral contributions to the signal at  $t$

$=0.0$  ps for both states  $|1\rangle$  and  $|2\rangle$  using the phase mask of Fig. 5(a). The overall line shape for state  $|1\rangle$  only partially reflects the  $1/\delta$  behavior expected from Eq. (3), but it unambiguously shows an increase in the contributing bandwidth. The increase in effective bandwidth is attributed to the application of  $\pm\pi/2$  phase to positively and negatively detuned frequencies. The spectral asymmetry is a result of a combination of diffraction effects in the SLM and an asymmetric laser pulse spectrum. The spectral contributions to the signal at  $t=0.0$  ps for state  $|2\rangle$  similarly show that there is an increase in the contributing bandwidth relative to the long time delay. More interestingly, the results show that blocking the resonant wavelength actually increases the signal at  $t=0.0$  ps, indicating a destructive interference. Even though the line shape remains ambiguous, the increase in signal relative to the baseline obtained by blocking the resonant frequency on pixel 74 is unambiguous. Since the wave-packet signal at long times consists of oscillations with a phase offset of approximately zero, the resonant contribution to the signal can be concluded to have a positive sign relative to state  $|1\rangle$ . This suggests that the total wave-function coefficient for state  $|2\rangle$  around  $t=0.0$  is negative, in agreement with the wave-packet phase data.

The results can be quantified in terms of the  $Z$ -gate representation as in Eq. (4), with the initial state taken to be the superposition at  $t=0.0$  ps, and the final state taken to be the superposition at  $t=\infty$ :

$$\begin{bmatrix} c_1(f) \\ c_2(f) \end{bmatrix} = \begin{bmatrix} \frac{C_{\text{res}_1}(\infty)}{C_{\text{res}_1}(0) + C_{\text{nonres}_1}(0)} & C_{\text{nonres}_{12}} \\ C_{\text{nonres}_{21}} & \frac{C_{\text{res}_2}(\infty)}{C_{\text{res}_2}(0) - C_{\text{nonres}_2}(0)} \end{bmatrix} \times \begin{bmatrix} c_1(i) \\ c_2(i) \end{bmatrix}, \quad (5a)$$

where  $C_{\text{res}_i}(t)$  and  $C_{\text{nonres}_i}(t)$  are the resonant and nonresonant contributions to the coefficient of state  $i$  at time  $t$ . The observed dynamics occur under weak-field excitation, so the launch-state contribution to the wave function dominates—excited-state dynamics only weakly affect the bulk of the launch-state wave function. Since the excited states are coupled only through the large-amplitude launch-state wave function, the off-diagonal elements between the excited-state coefficients of Eq. (5a),  $C_{\text{nonres}_{12}}$  and  $C_{\text{nonres}_{21}}$ , are very small. Because the direct coupling between excited states is very small, the maximum of the off-diagonal elements is defined here as the degree to which nonresonant control of one excited state affects the dynamics of the other.

The  $Z_{11}$  and  $Z_{22}$  elements of Eq. (5a) can be taken directly from the experimental data. The first diagonal  $Z_{11}$  element is determined to be 0.71, based upon the data from Fig. 2, where the ratio of excited-state populations is given as

$$\frac{|c_1(t=\infty)|^2}{|c_1(t=0)|^2} = 0.71^2. \quad (5b)$$

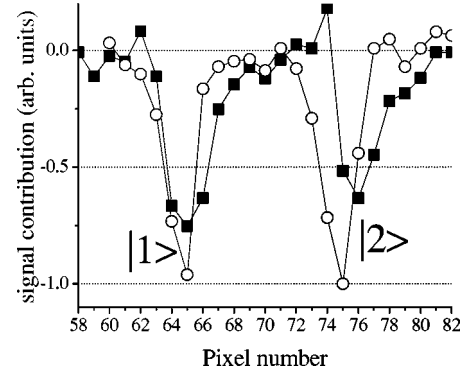


FIG. 7. Spectral contributions for shaped and unshaped pulses. The light on one pixel at a time is attenuated; the photoionization is plotted versus attenuated pixel. The amount of change in photoionization has been normalized. The  $\circ$  is the total photoionization change for an unshaped pulse at a fixed pump-probe delay of greater than 6.0 ps. The observed linewidths represent the resolution of the pulse shaper. The  $\blacksquare$  show the photoionization change for the phase mask of Fig. 5(a) at a fixed pump-probe delay of 0.0 ps. The  $\blacksquare$  spectrum around pixel 65 shows the effect of adding resonant and nonresonant contributions, and that around 75 represents subtracting resonant from nonresonant. Note the increased linewidth in the shaped pulse case, and the increase in signal while blocking pixel 74.

This matrix element is programmed to be less than 1 in the interest of simplifying the applied phase masks. The  $Z_{22}$  element can be determined from the coherent oscillation amplitude shown in Fig. 5. At long time delays, the peak-to-peak amplitude of the coherent oscillation is approximately 0.9 times that around  $t=0$ , or

$$\frac{|c_1(t=\infty)||c_2(t=\infty)|}{|c_1(t=0)||c_2(t=0)|} = 0.9. \quad (5c)$$

Given that  $|c_1(t=\infty)| \approx 0.71|c_1(t=0)|$ , then substitution of Eq. (5b) into Eq. (5c) leaves the relation that  $|c_2(t=\infty)| \approx 1.3|c_2(t=0)|$ . Using the wave-packet phase information of Fig. 4, this leaves a value of  $-1.3$  for the  $Z_{22}$  element of the  $Z$ -gate matrix, leaving an experimental transformation of the transiently prepared state at  $t=0$  ps:

$$\begin{bmatrix} c_1(f) \\ c_2(f) \end{bmatrix} = \begin{bmatrix} 0.7 \pm 0.1 & < 0.1 \\ < 0.1 & -1.3 \pm 0.2 \end{bmatrix} \begin{bmatrix} c_1(t=0) \\ c_2(t=0) \end{bmatrix}. \quad (5d)$$

The  $Z_{12}$  and  $Z_{21}$  elements  $C_{\text{nonres}_{12}}$  and  $C_{\text{nonres}_{21}}$  represent an upper limit to the switching of population from one state to another due to nonresonant Rabi oscillations and have previously been quantified with respect to the resonant contribution to the coefficients [24].

In the experimental  $Z$ -gate matrix, the error bars are given in terms of the absolute amplitude of the matrix elements. An additional uncertainty in the phase of the complex values of these matrix elements also needs to be considered. Ideally, as long as a phase of  $\pm\pi/2$  is applied to the various nonresonant contributions to the wave packet, there will only be an addition or subtraction of those components relative to resonance, so the imaginary component of the matrix elements in

this case can be assumed to be small. In other words, all contributions to the signal have been manipulated to have phases of either zero or  $\pi$ , which lie along the real axis of the complex plane. Experimentally, error in the measurement of the instantaneous phase implies a minimum measurable uncertainty of  $\pm 0.14\pi$  rad off the real axis, but pulse-shaping limitations (see Fig. 6) show that the true error can be larger.

The operations described here act upon a transient superposition with a large population in  $|0\rangle$ , with implications for multiple pulse sequences and reversibility. At times before  $t=0$ , the engineered pulse shapes create a superposition by exciting the two excited-state resonances. After  $t=0$ , the part of the electric field that excites  $|1\rangle$  is constructed to induce little net effect, but the part that excites  $|2\rangle$  undergoes a  $\pi$  phase shift. Since the population in  $|0\rangle$  is large and approximately constant compared to the excited state, the electric field after  $t=0$  destructively interferes with the previously prepared population in  $|2\rangle$ . This depopulates and then repopulates  $|2\rangle$  with a  $\pi$  phase shift relative to the initial superposition. In essence, the mechanism behind the phase changes in the superposition is that population from  $|0\rangle$  gets added to the excited-state superposition with varying phase at different points in time to overwhelm the previous excited-state superposition. If a second engineered pulse were to follow at a later time, the final excited-state amplitudes would essentially be doubled due to the parts of the pulse that come before  $t=0$ , illustrating the limitations of reversibility and of using this pulse-shaping scheme for computations.

The instantaneous wave-function phase could be better controlled and determined if the energy spacing between states were greater. First, the ability to control one state versus another increases as the state spacing increases as a result of the intrinsic  $1/\delta$  Rabi oscillation amplitude [24]. Next, the interference between  $|1\rangle$  and  $|2\rangle$  permits effective viewing of

the phase of state  $|2\rangle$ , but only at the maxima and minima of the interference signal, giving a data point every  $2/\omega_{12}$  ps, where the state spacing  $\omega_{12}$  is given in units of THz. With the current state spacing of  $42\text{ cm}^{-1}$ , one data point is retrieved every 0.3 ps, which is nearly half of the time scale over which the phase of state  $|2\rangle$  changes from  $\pi$  to 0 rad. Increasing the state spacing, or increasing the coherent oscillation frequency, will provide a more accurate probe for how the phase change occurs. Finally, a more rapid coherent oscillation will provide a more accurate measure of the amplitude of the coherent oscillation.

In this article, we outlined a system for manipulating the sign of one state in a two-state superposition while keeping the sign of the second state constant. We showed that this can be done by simply using weak-field, phase-shaped ultrafast pulses. Additionally, we have shown, using established spectral techniques, that the resonant and nonresonant contributions to a specific transition can be programmed to add together or to work in opposition on short time scales. This work expands upon established methods for controlling transient processes in molecular systems and presents a case where both the phase and amplitude of an excited state depend upon more than resonant frequencies.

#### ACKNOWLEDGMENTS

The authors gratefully acknowledge the support of the National Science Foundation, through the Chemistry Division and Information Technology Research. Portions of the included work were completed at the University of California, Berkeley, with some equipment on loan from the National Institute of Standards and Technology, Boulder, CO. L.H. would like to thank JILA for its hospitality and financial assistance.

- 
- [1] A. P. Peirce, M. A. Dahleh, and H. Rabitz, *Phys. Rev. A* **37**, 4950 (1988).
  - [2] M. Shapiro and P. Brumer, *J. Chem. Phys.* **84**, 4103 (1986).
  - [3] R. Bartels, S. Backus, E. Zeek, L. Misoguti, G. Vdovin, I. P. Christov, M. M. Murnane, and H. C. Kapteyn, *Nature (London)* **406**, 164 (2000).
  - [4] M. Gruebele and A. H. Zewail, *J. Chem. Phys.* **98**, 883 (1993).
  - [5] N. F. Scherer, D. M. Jonas, and G. R. Fleming, *J. Chem. Phys.* **99**, 153 (1993).
  - [6] J. Cao, C. J. Bardeen, and K. R. Wilson, *J. Chem. Phys.* **113**, 1898 (2000).
  - [7] H. Rabitz, R. d. Vivie-Riedle, M. Motzkus, and K. Kompa, *Science* **288**, 824 (2000).
  - [8] A. N. Naumov, A. Materny, W. Kiefer, M. Motzkus, and A. M. Zheltikov, *Laser Phys.* **11**, 1319 (2001).
  - [9] E. Biolatti, R. C. Iotti, P. Zanardi, and F. Rossi, *Phys. Rev. Lett.* **85**, 5647 (2000).
  - [10] C. M. Tesch and R. de Vivie-Riedle, *Phys. Rev. Lett.* **89**, 157901 (2002).
  - [11] Z. Amitay, R. Kosloff, and S. R. Leone, *Chem. Phys. Lett.* **359**, 8 (2002).
  - [12] J. Ahn, C. Rangan, D. N. Hutchinson, and P. H. Bucksbaum, *Phys. Rev. A* **66**, 022312 (2002).
  - [13] Z. Bihary, D. R. Glenn, D. A. Lidar, and V. A. Apkarian, *Chem. Phys. Lett.* **360**, 459 (2002).
  - [14] M. A. Nielsen and I. L. Chuang, *Quantum Computation and Quantum Information* (Cambridge University Press, Cambridge, England, 2000).
  - [15] D. P. DiVincenzo, D. Bacon, J. Kempe, G. Burkhard, and K. B. Whaley, *Nature (London)* **408**, 339 (2000).
  - [16] M. N. Leuenberger and D. Loss, *Nature (London)* **410**, 789 (2001).
  - [17] N. A. Gershenfeld and I. L. Chuang, *Science* **275**, 350 (1997).
  - [18] J. A. Jones and M. Mosca, *J. Chem. Phys.* **109**, 1648 (1998).
  - [19] J. I. Cirac and P. Zoller, *Phys. Rev. Lett.* **74**, 4091 (1995).
  - [20] D. Kielpinski, C. Monroe, and D. J. Wineland, *Nature (London)* **417**, 709 (2002).
  - [21] R. Uberna, M. Khalil, R. M. Williams, J. M. Papanikolas, and S. R. Leone, *J. Chem. Phys.* **108**, 9259 (1998).
  - [22] J. B. Ballard, H. U. Stauffer, Z. Amitay, and S. R. Leone, *J. Chem. Phys.* **116**, 1350 (2002).
  - [23] D. Oron, N. Dudovich, D. Yelin, and Y. Silberberg, *Phys. Rev. Lett.* **88**, 063004 (2002).

- [24] J. B. Ballard, H. U. Stauffer, E. Mirowski, and S. R. Leone, *Phys. Rev. A* **66**, 043402 (2002).
- [25] R. Uberna, Z. Amitay, C. X. W. Qian, and S. R. Leone, *J. Chem. Phys.* **114**, 10 311 (2001).
- [26] N. Dudovich, B. Dayan, S. M. Gallagher Faeder, and Y. Silberberg, *Phys. Rev. Lett.* **86**, 47 (2001).
- [27] L. Allen and J. H. Eberly, *Optical Resonance and Two-Level Atoms* (Dover, New York, 1987).
- [28] R. A. Bernheim, L. P. Gold, and C. A. Tomczyk, *J. Chem. Phys.* **87**, 861 (1987).
- [29] I. Schmidt-Mink, W. Muller, and W. Meyer, *Chem. Phys.* **92**, 263 (1985).
- [30] M. M. Wefers and K. A. Nelson, *Opt. Lett.* **18**, 2032 (1993).
- [31] M. M. Wefers and K. A. Nelson, *J. Opt. Soc. Am. B* **12**, 1343 (1995).